Multifractality of instantaneous normal modes at mobility edges

B. J. Huang and Ten-Ming Wu*
Institute of Physics, National Chiao-Tung University, HsinChu, Taiwan 300, Republic of China
(Received 8 July 2010; revised manuscript received 7 October 2010; published 29 November 2010)

In terms of the multifractal analysis, we investigate the characteristics of the instantaneous normal modes (INMs) at two mobility edges (MEs) of a simple fluid, where the locations of the MEs in the INM spectrum were identified in a previous work [B. J. Huang and T. M. Wu, Phys. Rev. E **79**, 041105 (2009)]. The mass exponents and the singularity spectrum of the INMs are obtained by the box-size and system-size scalings under the typical average. The INM eigenvectors at a ME exhibit a multifractal nature and the multifractal INMs at each ME yield the same results in generalized fractal dimensions and singularity spectrum. Our results indicate that the singularity spectrum of the multifractal INMs agrees well with that of the Anderson model at the critical disorder. This good agreement provides numerical evidence for the universal multifractality at the localization-delocalization transition. For the multifractal INMs, the probability density function and the spatial correlation function of the squared vibrational amplitudes are also calculated. The relation between the probability density function and the singularity spectrum is examined numerically, so are the relations between the critical exponents of the spatial correlation function and the mass exponents of the multifractal INMs.

DOI: 10.1103/PhysRevE.82.051133 PACS number(s): 05.40.−a, 05.45.Df, 63.50.−x, 72.15.Rn

I. INTRODUCTION

The localization-delocalization transition (LDT) induced by disorder, also known as the Anderson transition, is at the forefront of physics and has been intensively studied with the model proposed by Anderson for the transport of noninteracting electrons [1]. Nowadays, the researches on this subject are more active than ever, since the LDT occurs in a broad range of physical systems related to waves [2–8]. In the Anderson model (AM), the amplitudes of the electronic wave functions at the LDT exhibit strong fluctuations characterized in a multifractal nature [9]. It is challenging to study the multifractality at the LDT by numerical methods, with which only finite-size systems are investigated. Owing to the recent advance in computers and algorithms, the AM has been calculated at much large scales [10–13] so that the understanding for the multifractality at the LDT has considerably progressed.

The LDT also happens to vibrational excitations, the waves of atomic motions, in disordered media [14–17]. The studies with vibrational excitations have the benefit to avoid the complicated problems occurring in the electronic systems due to the electron-electron and electron-phonon interactions, which make the electron transport in the real materials deviated from the AM. Vibrational modes in perfect lattices are extended and some localized modes appear as weak disorder is introduced by impurities or defects in lattices. In topologically disordered systems, such as amorphous materials, the strong disorder in atomic structures makes the systems no longer possess a reference of lattice. The vibrational modes in the topologically disordered systems are generally extended at low frequencies but localized in the high-frequency end of the vibrational spectrum, so that a LDT occurs at some vibrational frequency, named as mobility edge (ME). Expected to behave multifractally also, the vibrational modes at a ME provide an alternative for investigating the universality of the multifractals at the LDT. Recently, localization of ultrasound is observed in a three-dimensional elastic network of aluminum beads and the localized ultrasounds show strong multifractality [5,18].

We have recently identified the LDT in the instantaneous normal mode (INM) spectrum of a simple fluid [19]. Referred as the eigenmodes of the Hessian matrices calculated at the instantaneous configurations, the INMs of a fluid may have positive and negative eigenvalues since the fluid configurations are not necessary at the local minima of energy landscape [20]. By the level-spacing (LS) statistics and the approach of finite-size scaling, we find two MEs—one with a positive eigenvalue and the other with a negative eigenvalue—in the INM spectrum. Determined by the scale invariance of the nearest-neighbor LS distribution, the locations of the two MEs are confirmed by good agreement in the critical exponent and the nearest-neighbor LS distribution at each ME with those of the AM at the critical disorder. This confirmation is fulfilled with the requirement by the random matrix theory [21], which indicates that the LS statistics at a LDT is universal and subject to the universality class of the associated random matrices.

Although the universal features of the vibrational modes and the electronic eigenstates at the LDT were reported [17], the comparison in quantity between the multifractal natures of the vibrational modes and those obtained by the AM is lacking. In this paper, we calculate the multifractal properties at the MEs in the INM spectrum of the simple fluid we studied before and compare our results with those of the AM at the critical disorder. Since the two disordered systems are fundamentally different, this comparison serves a naive numerical examination for the universal multifractality at the LDT. In Sec. II, we describe how the fluid configurations are generated by simulations and present a visualization of the multifractal structures of the INMs at a ME. In Sec. III, we generalize the multifractal analysis for the INMs. In Sec. IV, by the standard box-counting method [22], we calculate the singularity spectrum of the multifractal INMs. Also, the

*tmw@faculty.nctu.edu.tw

TABLE I. The system sizes of our simulations for the TLJ fluid at $\rho^*=0.972$ and $T^*=0.836$. N is the particle number and $L=(N/\rho^*)^{1/3}$ is the length of simulation box. Both L and ρ^* are in the LJ units.

N	3000	6000	12000	24000	48000	96000
L	14.56	18.38	23.12	29.12	36.69	46.22

probability density function (PDF) and the spatial correlation function of the squared vibrational amplitudes in the multifractal INMs are investigated and their relations to the singularity spectrum and the mass exponents are examined. Our conclusions are given in Sec. V.

II. INMS AT MOBILITY EDGE

Using the Monte Carlo simulation for N particles in a cubic box of length L and the periodic boundary conditions, we generate the configurations of the truncated Lennard-Jones (TLJ) fluid at reduced density $\rho^*=0.972$ and reduced temperature $T^*=0.836$ in terms of the LJ units [23]. Given in Table I for the particle number N and the box length L, the simulations of six system sizes are performed.

With the definition given in Ref. [24], the Hessian matrices of the generated configurations are evaluated and then diagonalized with the JADAMILU package [25,26]. Presented in Fig. 2 of Ref. [19], the INM-eigenvalue spectrum $D(\lambda)$ consists of two branches, corresponding to the positive and negative eigenvalues. According to the results of the LS statistics for four system sizes between $N=3000$ and $N=24\,000$, the MEs are located at $\lambda_{pc}=1183.8\pm0.8$ and $\lambda_{nc}=-87.1\pm0.3$. By the multifractal analysis given below for system sizes up to $N=96\,000$ [15,27], the ME in the negative-eigenvalue branch is found at $\lambda_{nc}=-86.6\pm0.5$, which, within numerical errors, agrees with that obtained by the LS statistics.

For each configuration of N particles, there are $3N$ INMs with discrete eigenvalues λ_s, where the INM label s is from 1 to $3N$. For INM s, the $3N$ components of the normalized eigenvector are denoted as $\mathbf{e}_j^s$ for $j=1,\ldots,N$, where $\mathbf{e}_j^s$ is the three-dimensional projection vector of particle j in the INM [28]. The magnitude of the projection vector, $|\mathbf{e}_j^s|$, stands for the vibrational amplitude of particle j in INM s. Due to the normalization of an INM eigenvector, the vibrational amplitudes of all particles in an INM are subject to a sum rule,

$$\sum_{j=1}^{N} |\mathbf{e}_j^s|^2 = 1. \tag{1}$$

Generally, the geometric structure of an INM eigenvector can be represented by the spatial distribution of the vibrational amplitudes. A visualization for the vibrational amplitudes in an INM at the ME is shown in Fig. 1.

III. MULTIFRACTAL ANALYSIS FOR INMS

In this section, we generalize the multifractal analysis [29] for the INMs at the two MEs. We use the standard box-counting procedure, first dividing the simulation box into N_η small boxes of linear size l, where $N_\eta=\eta^{-3}$ with $\eta=l/L$. Because of the fluidity in our system, the particle number n in a small box of each realization fluctuates around the average value $n_0=N/N_\eta$. As shown in Fig. 2, for a small η, n_0 is very small so that a small variation of n from boxes to boxes causes a large fluctuation on the particle ratio n/n_0. The fluctuation of n is generally a result due to the topologically disordered structures in our model. This is one of the differences between our model and the AM, in which the numbers of lattice points in every small boxes in the box-counting procedure are the same. Thus, the box-counting procedure for our model is nothing but a coarse graining of our system from particles with a unit size into the small boxes by a scaling factor l in length.

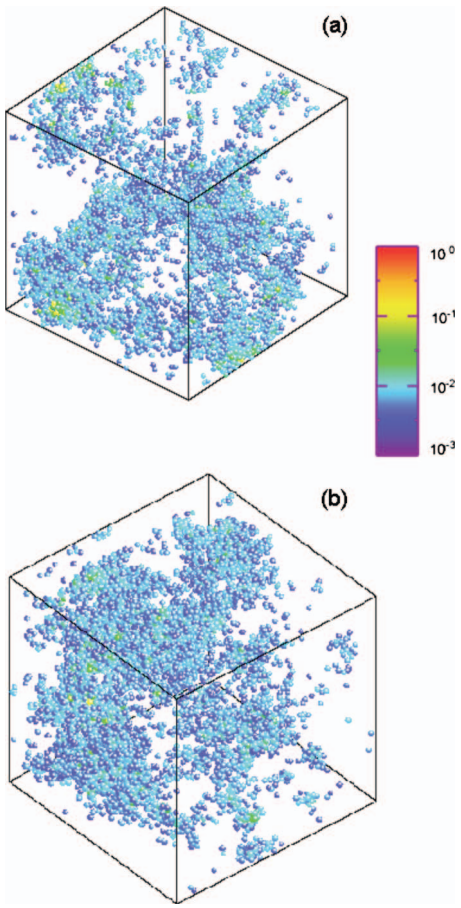

FIG. 1. (Color) Geometric structure of the INM with (a) $\lambda=1183.25$ or (b) -86.78 for the TLJ fluid of 96 000 particles in a box of $L=46.22$. In each panel, particles with vibrational amplitudes $|\mathbf{e}_i^s|$ larger than the average value $N^{-1/2}$ are presented by spheres with diameter of one and centered at particle position. The color of each sphere indicates the $|\mathbf{e}_j^s|$ value of the particle. The total numbers of spheres presented in (a) and (b) are about 5700 and 7000, respectively.

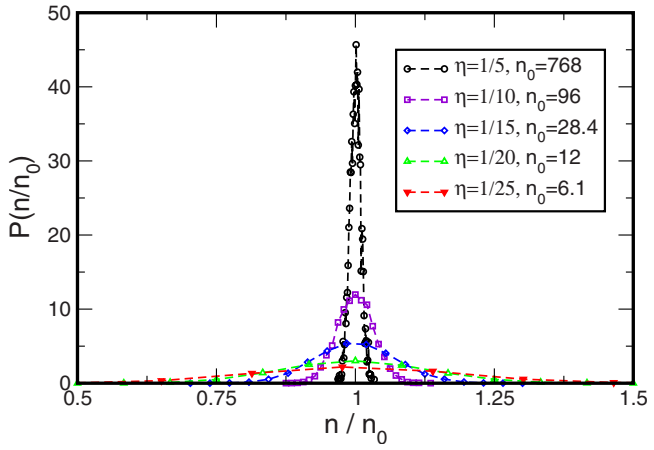

FIG. 2. (Color online) Distribution of particle number n in a small box in the box-counting method for the TLJ fluid of $N=96\,000$ particles. The symbols are the numerical results for several η values. $n_0=N/N_\eta$ is the average particle number of a small box.

Considering INM s of a configuration, we define a measure $\mu_k^s(\eta)$ as the sum of the squared vibrational amplitudes of particles inside the kth small box with the expression as

$$\mu_k^s(\eta) = \sum_{j \in box k} |\mathbf{e}_j^s|^2. \tag{2}$$

The generalized inverse participation ratio $P_q^s(\eta)$ of this INM is defined as a summation of the qth moment of $\mu_k^s(\eta)$ over all small boxes. That is,

$$P_q^s(\eta) = \sum_{k=1}^{N_\eta} [\mu_k^s(\eta)]^q. \tag{3}$$

Due to the normalization condition in Eq. (1), as $q=1$, $P_q^s(\eta)=1$ for all INMs and all values of η. Then, we make a typical average on $P_q^s(\eta)$ over the INMs within a small eigenvalue window [11,29,30]. The typical average of $P_q^s(\eta)$, denoted as $P_q(\lambda,\eta)$, is defined as

$$P_q(\lambda,\eta) \equiv \exp < \ln P_q^s(\eta) >_\lambda, \tag{4}$$

where $\langle \cdots \rangle_\lambda$ is an arithmetic average over the INMs with eigenvalues within a small interval of width $\Delta\lambda$ and centered at λ.

Underlying the assumption of multifractality, which, in principle, has no relevant length scale, $P_q(\lambda,\eta)$ is assumed to follow the power-law behavior

$$P_q(\lambda,\eta) \propto \eta^{\tau_q}. \tag{5}$$

From this scaling relation, τ_q is given as

$$\tau_q = \lim_{\eta \to 0} \frac{\ln P_q(\lambda,\eta)}{\ln \eta}. \tag{6}$$

The mass exponent τ_q is a quantity characterizing the nature of the INMs under the average: $\tau_q=d(q-1)$ for the delocalized INMs, where d is the space dimension and $\tau_q=0$ for the localized INMs. At the MEs, $\tau_q=D_q(q-1)$, where D_q is the so-called generalized fractal dimension. Generally, D_q depends only on the universality class of the associated random matrices so that D_q should be the same for the two MEs in the INM spectrum. The value of D_q is less or larger than d for positive or negative q, respectively.

In the multifractal analysis, the singularity spectrum $f(\alpha)$ is a useful quantity, which can be obtained from τ_q through a Legendre transformation,

$$f_q = f(\alpha_q) = \alpha_q q - \tau_q, \tag{7}$$

with

$$\alpha_q = \frac{d\tau_q}{dq}, \quad q = f'(\alpha). \tag{8}$$

The meaning of $f(\alpha)$ for the INMs is given as the following: as long as the scaled linear size $L'=1/\eta$ is large enough, the small boxes, which are specified with the coarse-grain squared vibrational amplitudes $\mu_k^s(\eta)$ scaled as η^α, form a fractal with a fractal dimension $f(\alpha)$. That is, the number of such small boxes scales as $L'^{f(\alpha)}$. Alternatively, by considering directly the particles in the fluid configuration of linear size L, $f(\alpha)$ is the fractal dimension of the set of particles with $|\mathbf{e}_j^s|^2 \sim L^{-\alpha}$ and, thus, the number of such particles scales as $L^{f(\alpha)}$. In the typical average, the behavior of $P_q(\lambda,\eta)$ is generally dominated by a single representative INM [30]. To make sure that the particle number scaling as $L^{f(\alpha)}$ in the representative INM is always larger than one, $f(\alpha)$ under the typical average is always positive [11] no matter what the value of L is.

According to the definitions given in Eqs. (7) and (8) and τ_q in Eq. (6), α_q and f_q can be reformulated as the following expressions:

$$\alpha_q = \lim_{\eta \to 0} \frac{\ln T_q(\lambda,\eta)}{\ln \eta}, \tag{9}$$

$$f_q = \lim_{\eta \to 0} \frac{\ln F_q(\lambda,\eta)}{\ln \eta}, \tag{10}$$

where

$$\ln T_q(\lambda,\eta) = \left\langle \sum_{k=1}^{N_\eta} \delta_k^s(q,\eta) \ln \delta_k^s(1,\eta) \right\rangle_\lambda, \tag{11}$$

$$\ln F_q(\lambda,\eta) = \left\langle \sum_{k=1}^{N_\eta} \delta_k^s(q,\eta) \ln \delta_k^s(q,\eta) \right\rangle_\lambda, \tag{12}$$

with $\delta_k^s(q,\eta) \equiv [\mu_k^s(\eta)]^q / P_q^s(\eta)$. With the sets of α_q and f_q calculated by Eqs. (9) and (10) for different values of the implicit parameter q, the function of $f(\alpha)$ under the typical average is obtained such that the difficulties in numerical calculations via Eqs. (7) and (8) are avoided.

IV. MULTIFRACTALITY OF INMs AT A ME

In this section, we present the multifractal properties of the INMs at the MEs, including the generalized fractal dimension and the singularity spectrum. We also show the probability density function and the spatial correlation function of squared vibrational amplitudes in the multifractal

INMs. The results presented in the following are averaged for the INMs with $\lambda=-86.6\pm0.5$ or those with $\lambda=1183.8\pm1$.

A. Fractal dimension and singularity spectrum

The thermodynamic limit in Eq. (6) is achieved by either $L\to\infty$ or $l\to0$ but, practically, these two limits cannot be obtained numerically for the discrete nature of our model due to particle size and the finite sizes of simulated systems. Instead of taking the limit, the value of τ_q is interpreted as the slope of $\ln P_q(\lambda,\eta)$ versus $\ln\eta$ as η is very small. Hence, this slope can be obtained numerically by a linear fit of the $\ln P_q(\lambda,\eta)$ data within a finite interval of η. Similarly, the values of α_q and f_q in Eqs. (9) and (10) are obtained from the slope of a linear fit for $\ln T_q(\lambda,\eta)$ and $\ln F_q(\lambda,\eta)$ versus $\ln\eta$, respectively. By this approach, the three quantities versus $\ln\eta$ can be calculated in two different ways: the box-size scaling and the system-size scaling. In the box-size scaling, only one system with very large L is needed so that L is a constant and the variations of the three measured quantities with the box-size l are calculated. In the system-size scaling, all simulated systems with different L are partitioned into small boxes of the same size so that l is a constant and the variations of the measured quantities with L are evaluated.

In the box-size scaling, by averaging 5×10^3 INM eigenvectors of $N=96\,000$ at the ME in the negative branch and taking the scaled size $L'=1/\eta$ as an integer varied from 2 to 10, we have calculated $\ln P_q(\lambda,\eta)$, $\ln T_q(\lambda,\eta)$, and $\ln F_q(\lambda,\eta)$ for q between -5 and 5. The numerical results of integer q are presented in Fig. 3, including the linear fit for the data of each q. Generally, for each q, the $\ln P_q(\lambda,\eta)$, $\ln T_q(\lambda,\eta)$, and $\ln F_q(\lambda,\eta)$ data have a linear behavior at small $\ln\eta$. We have performed the same calculations at the positive-eigenvalue ME and the results are almost the same as those in Fig. 3.

In system-size scaling, we set $l=2.427$ such that the simulated system of $N=3000$ is exactly partitioned into 216 boxes, with $L'=6$ and the average particle number $n_0=13.9$. For other larger simulated systems and with this l, L/l is not exactly an integer so that we partition each realization into small boxes of size l as many as possible, with some remains not enough to be a small box. In such a partition, the number of small boxes available is $\tilde{L}^3$, where $\tilde{L}$ is the maximum integer which is smaller than or equal to L/l. Thus, for the six system sizes that we have simulated, the values of $\tilde{L}$ are 6, 7, 9, 12, 15, and 19; correspondingly, the definition of η in the system-size scaling changes as $1/\tilde{L}$. For a partition with remains, only particles in those small boxes are involved in the calculations of $\mu_k^s(\eta)$; however, by requiring that one corner of the partitioned box of size $\tilde{L}$ coincides with one of the simulation box, each realization may have eight different ways of partition, which enhances the number of sampling for statistical average. Calculated with the system-size scaling, the results of $\ln P_q(\lambda,\eta)$, $\ln T_q(\lambda,\eta)$, and $\ln F_q(\lambda,\eta)$ versus $\ln\eta$ are close to those shown in Fig. 3.

The mass exponent τ_q and the generalized fractal dimension $D_q=\tau_q/(q-1)$ at the two MEs are plotted in Fig. 4 for

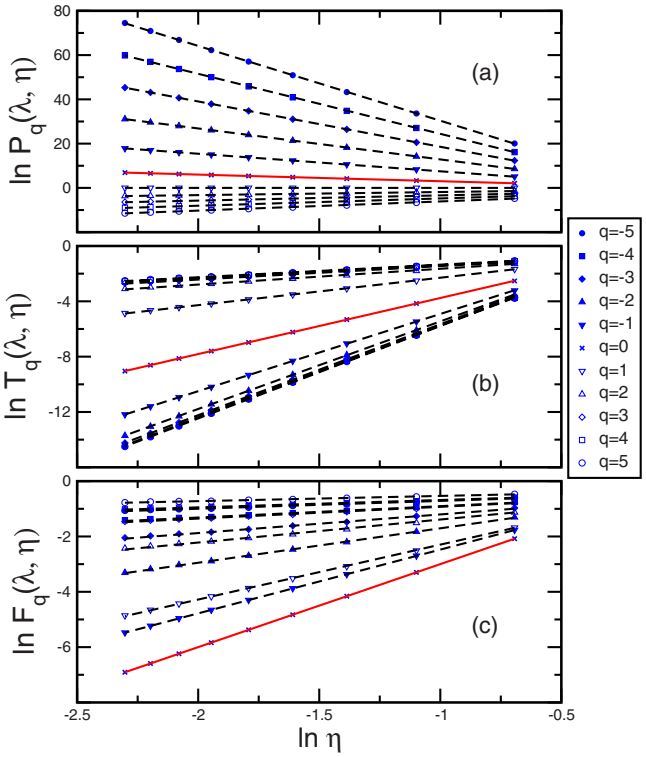

FIG. 3. (Color online) (a) $\ln P_q(\lambda,\eta)$, (b) $\ln T_q(\lambda,\eta)$, and (c) $\ln F_q(\lambda,\eta)$ versus $\ln\eta$ for the INMs with $\lambda=-86.6\pm0.5$. The numerical data are obtained by the box-size scaling for $N=96\,000$, with the scaled size $L'=1/\eta$ an integer from 2 to 10. The symbols are the numerical results, with the filled ones for negative q, the open ones for positive q, and the crosses for $q=0$. The data errors are smaller than the symbol size. The linear fits for the data are indicated by either the black dashed lines for $q\neq0$ or the red solid line for $q=0$.

$-5\le q\le5$. The data obtained by the box-size scaling are accurate enough to indicate that τ_q and D_q at the two MEs are identical. At $q=0$, $\tau_q=-d$ and $D_q=0$ as expected. For $q=2$, D_2 is the correlation dimension of the inverse participation ratio P_2 [28,30,31]. The results of the box-size scaling give $D_2=1.40\pm0.03$, which is generally comparable with the D_2 value of the AM estimated with the previously reported methods [32–35]. However, the value of D_2 by the system-size scaling is 1.29 ± 0.04, close to the value reported recently by the generalized multifractal analysis for the AM [36]. In principle, as q varies from $-\infty$ to ∞, τ_q is a monotonically increase function of q, but the slope of the function, which is α_q, decreases from the limiting value α_+ to α_-, which confines the range of the singularity spectrum $f(\alpha)$ under the typical average [11]. Estimated by our data at $|q|=5$ in Fig. 4(a), the value of α by the box-size scaling is limited from 0.86 to 6.7; with almost the same upper limit, the range of α by the system-size scaling is extended to 0.78.

Presented in the insets of Figs. 5(a) and 5(b) are the values of α_q and f_q generated from the slope of the linear fit for $\ln T_q(\lambda,\eta)$ and $\ln F_q(\lambda,\eta)$ with $-5\le q\le5$, respectively. With the α_q and f_q data by the box-size scaling, the singularity spectra $f(\alpha)$ at the two MEs are plotted in Fig. 5(a). Within numerical errors, the singularity spectra at the two

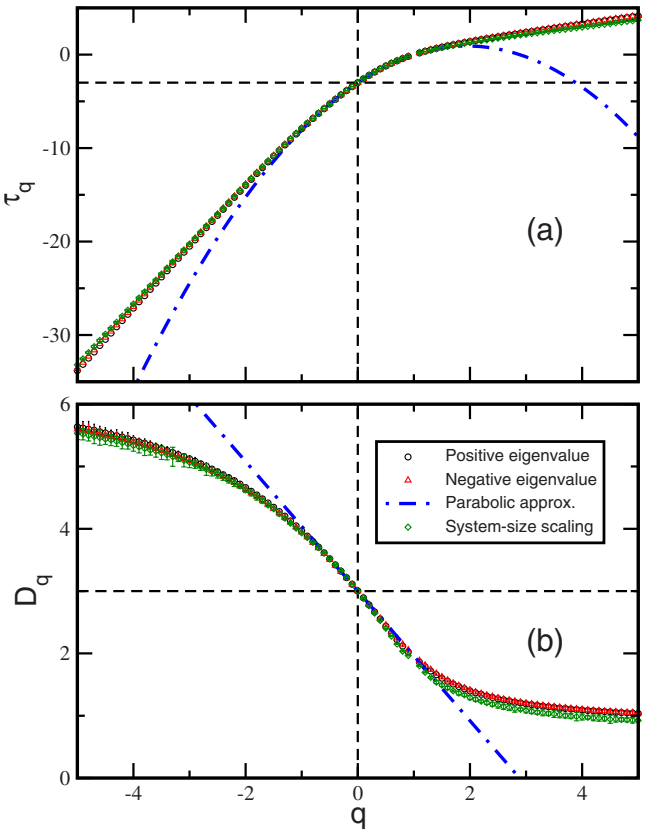

FIG. 4. (Color online) (a) Mass exponent τ_q and (b) generalized fractal dimension D_q as a function of q. The black circles and red triangles are obtained by the box-size scaling for INMs with $\lambda = 1183.8 \pm 1.0$ and $\lambda = -86.6 \pm 0.5$, respectively. The green diamonds are obtained by the system-size scaling for INMs with $\lambda = -86.6 \pm 0.5$. The data errors in (a) and those around $q=0$ in (b) are smaller than the symbol size. The dashed-dotted lines are the PA with $\alpha_0 = 4.04$.

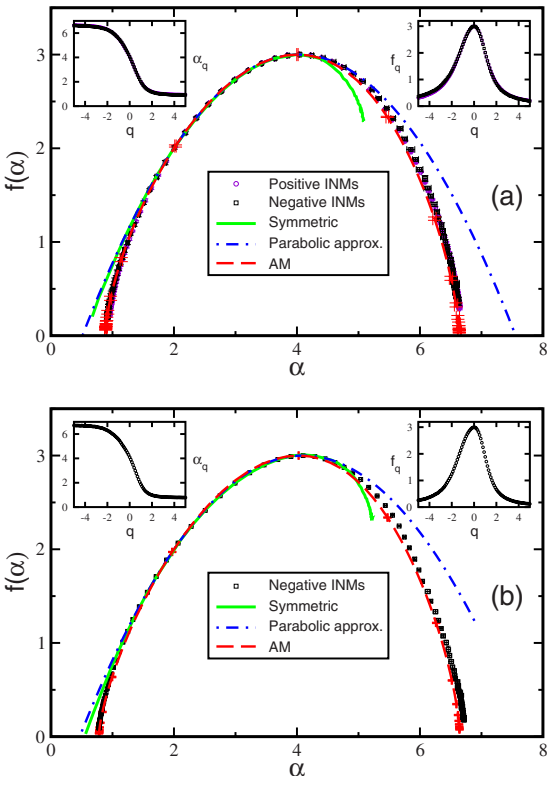

FIG. 5. (Color online) Singularity spectrum $f(\alpha)$ of the INMs at a ME obtained by (a) the box-size scaling and (b) the system-size scaling. In (a), the INMs are calculated with $\lambda = 1183.8 \pm 1$ (circles) and $\lambda = -86.6 \pm 0.5$ (squares) for $N = 96\,000$; in (b), the INMs with $\lambda = -86.6 \pm 0.5$ (squares) are calculated for six system sizes from $N = 3000$ to 96 000. In each panel, $f(\alpha)$ is generated with the data of α_q and f_q shown in the insets for $-5 \le q \le 5$ with a step of $\Delta q = 0.1$. The green solid line is the corresponding spectrum transformed via the symmetric relation in Eq. (17). The red dashed line is that of the AM at the critical disorder [11]. The blue dashed-dotted lines in (a) and (b) are the PA with $\alpha_0 = 4.04$ and $\alpha_0 = 4.10$, respectively.

MEs are generally identical and also agree with that of the AM at the critical disorder [11]. This agreement provides another confirmation for the locations of the two MEs in the INM spectrum. Indicated by our results, the maximum of $f(\alpha)$ occurs at $\alpha_0 = 4.034 \pm 0.006$ for the positive-eigenvalue ME and $\alpha_0 = 4.049 \pm 0.016$ for the negative-eigenvalue ME; the two values of α_0 generally agree with each other. Similarly, with the data of the system-size scaling, the singularity spectrum at the negative-value ME is presented in Fig. 5(b), with $\alpha_0 = 4.1 \pm 0.02$ and the left end of the spectrum extended toward smaller α as compared with the one obtained by the box-size scaling. The singularity spectrum generally agrees with that of the AM obtained by the system-size scaling [11], except for a small deviation in the right (large α) end, which is attributed to the small average particle number and large fluctuations in the small boxes in our system-size-scaling calculations.

Around the maximum at α_0, where $f(\alpha_0) = d$, the singularity spectrum can be described by Wegner's parabolic approximation (PA) [37],

$$f^{\mathrm{PA}}(\alpha) = d - \frac{(\alpha - \alpha_0)^2}{4(\alpha_0 - d)}, \tag{13}$$

which is ensured to go through the maximum of $f(\alpha)$ and to be tangential to the line $f(\alpha) = \alpha$. As shown in Figs. 5(a) and 5(b), $f(\alpha)$ deviates from the PA as α is near either α_+ or α_-, and the overall shape of $f(\alpha)$ becomes asymmetric about the maximum of $f(\alpha)$.

By substituting $f(\alpha)$ in Eqs. (7) and (8) with $f^{\mathrm{PA}}(\alpha)$, τ_q and D_q under the PA are given as

$$\tau_q^{\mathrm{PA}} = -(\alpha_0 - d)q^2 + \alpha_0 q - d, \tag{14}$$

$$D_q^{\mathrm{PA}} = -(\alpha_0 - d)q + d, \tag{15}$$

where α_0 is the only parameter. By setting $\alpha_0 = 4.04$, τ_q^{PA} and D_q^{PA}, as shown in Fig. 4, are good only for small q.

Relative to the fully delocalized states, the anomalous dimension of multifractals is defined as $\Delta_q \equiv \tau_q - d(q-1)$. Recently, based on the nonlinear σ model [10,38,39], a symmetric relation of the anomalous dimension is shown as

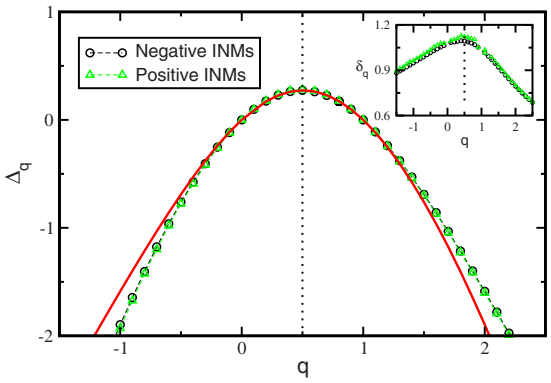

FIG. 6. (Color online) Anomalous dimension Δ_q and reduced anomalous dimension δ_q (inset) versus q at a ME. Obtained by the box-size scaling, the circles and triangles, guiding the eye with the dashed line, are the Δ_q data of the INMs with $\lambda=-86.6\pm0.5$ and 1183.8 ± 1, respectively. The data errors are smaller than the symbol size. The red solid line is the mirror image of the Δ_q data with respect to the line $q=1/2$.

$$\Delta_q = \Delta_{1-q}. \tag{16}$$

With the symmetric relation of Δ_q, it has been proved that the $f(\alpha)$ value for $\alpha<d$ and that for $\alpha>d$ are transformed with each other via the relation

$$f(2d-\alpha) = f(\alpha) + d - \alpha, \tag{17}$$

where α is only defined between 0 and $2d$. The symmetric relation of Δ_q has been confirmed numerically for the power-law random banded matrix model in one dimension [10], the symplectic Anderson model in two dimensions [40] and the orthogonal Anderson model in three dimensions [11,12] and evidenced experimentally by the ultrasound waves in two dimensions [18].

We also show in Figs. 5(a) and 5(b) the comparison between the singularity spectrum of the INMs and the one generated via the symmetric relation in Eq. (17). By the box-size scaling, $f(\alpha)$ at a ME is generally satisfied with the symmetric relation within $2\leq\alpha\leq4$, which is similar as the range for the AM. To examine the symmetric relation of Δ_q for the INMs at a ME, we plot in Fig. 6 the anomalous dimension Δ_q and compare Δ_q with Δ_{1-q}, which is obtained by the mirror image of Δ_q with respect to $q=1/2$. Our data of Δ_q at each ME are satisfied with the symmetric relation for q between -0.5 and 1.5. Shown in the inset in Fig. 6 is the reduced anomalous dimension $\delta_q=\Delta_q/q(1-q)$. Our result of δ_q versus q has a similar shape as the one measured by the multifractal ultrasounds on the surface of an elastic network [18].

According to our results, we have shown that the INMs at the MEs behave in the same multifractal features as those of the lattice AM at the critical disorder. The agreement between our results and those of the AM gives a numerical evidence for the universality of multifractals at a LDT. In the following, we investigate the vibrational amplitudes in the multifractal INMs and present only the results at the ME in the negative branch.

B. Probability density function

Another approach to characterize the multifractal INMs is the statistics of squared vibrational amplitudes in individual INM eigenvector. Averaged over the multifractal INMs of N particles in a system of size L, the PDF $\tilde{P}_L(\psi)$ of the squared vibrational amplitudes $\psi=|\mathbf{e}_j^s|^2$ is defined such that $\tilde{P}_L(\psi)\Delta\psi$ is the ratio $\Delta N/N$, where ΔN is the averaged number of particles with squared vibrational amplitudes lying between ψ and $\psi+\Delta\psi$ in an INM. By changing variable to the singularity strength $\alpha=-\ln\psi/\ln L$, the corresponding PDF $P_L(\alpha)$ is given as $\tilde{P}_L(\psi)d\psi/d\alpha$. Based on the physical meaning of $f(\alpha)$, $P_L(\alpha)$ has a scaling of $L^{f(\alpha)-d}$. Recently, it has been proved analytically and confirmed with the numerical results of the AM in three dimensions [13] that the proportionality of the scaling is the maximum value of the PDF at α_0 because of $f(\alpha_0)=d$. Thus, $P_L(\alpha)$ can be expressed as

$$P_L(\alpha) = P_L(\alpha_0)L^{f(\alpha)-d}. \tag{18}$$

Since the scale invariance of α_0 with system size, the position of the maximum PDF is expected to be independence of L.

By using the PA of $f(\alpha)$ in Eq. (13), we obtain a Gaussian approximation (GA) of $P_L(\alpha)$ as

$$P_L^{\mathrm{GA}}(\alpha) = P_L(\alpha_0)\exp\left\{-\frac{(\alpha-\alpha_0)^2}{4(\alpha_0-d)}\ln L\right\}. \tag{19}$$

Under the GA, the distribution width of $P_L(\alpha)$ decreases with $(\ln L)^{1/2}$, while the maximum $P_L(\alpha_0)$ increases with $(\ln L)^{1/2}$ due to the normalization of the PDF. On the other hand, in terms of the symmetric relation of $f(\alpha)$ in Eq. (17), $P_L(\alpha)$ for large enough L is expected to approach the one generated via the symmetric transformation (ST),

$$P_L^{\mathrm{ST}}(\alpha) = L^{\alpha-d}P_L(2d-\alpha), \tag{20}$$

where $0\leq\alpha\leq2d$. The equivalence of $P_L(\alpha)$ and $P_L^{\mathrm{ST}}(\alpha)$ implies that the values of $P_L(\alpha\geq d)$ and $P_L(d\leq\alpha)$ are correlated with each other. Therefore, the investigation of $P_L(\alpha)$ provides an insight into the property of $f(\alpha)$.

Calculated with 7000 INM eigenvectors for each N from 3000 to 96 000, the variation of $P_L(\alpha)$ with system size is shown in Fig. 7. Located at $\alpha=4.1\pm0.04$, the position of the $P_L(\alpha)$ maximum is almost invariant with system size. Within our numerical resolution, this maximum position is very close to the α_0 value of $f(\alpha)$ obtained by the system-size scaling in Fig. 5(b). Shown in the inset of Fig. 7, $P_L(\alpha_0)$, with $\alpha_0=4.1$, indeed scales as $(\ln L)^{1/2}$, which agrees with the prediction of the GA.

The comparisons of $P_L(\alpha)$ with $P_L^{\mathrm{GA}}(\alpha)$ and $P_L^{\mathrm{ST}}(\alpha)$ are shown in Fig. 8(a) for $N=96\,000$. Our results indicate that a noticeable deviation of $P_L(\alpha)$ from the GA or the ST is found in the large-α region, which corresponds to small vibrational amplitudes. To quantify the deviation of $P_L(\alpha)$ from the GA or the ST, we define the difference $\delta P_L^O(\alpha)=P_L(\alpha)-P_L^O(\alpha)$, where O is either GA or ST and the integrated difference $\delta P_L^O=\int_0^{\alpha_c}|\delta P_L^O(\alpha)|d\alpha$, where $\alpha_c=2d$ for $O=$ST and $\alpha_c=7$ for $O=$GA. The numerical results of $\delta P_L^O(\alpha)$ are presented in Fig. 8(b) and the system-size dependences of δP_L^{ST} and δP_L^{GA}

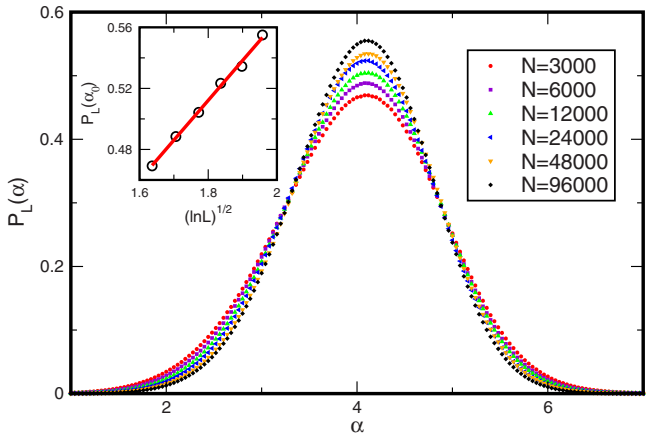

FIG. 7. (Color online) System-size dependence of $P_L(\alpha)$ for INMs with $\lambda=-86.6\pm0.5$. $\alpha=-\ln|\mathbf{e}_j^s|^2/\ln L$. The symbols denote the numerical results with a resolution $\Delta\alpha=0.04$. With $\alpha_0=4.10$, the inset shows $P_L(\alpha_0)$ versus $(\ln L)^{1/2}$ and the fit of $A+B(\ln L)^{1/2}$ (red solid line), with $A=0.043$ and $B=0.261$.

are in the inset of the figure. For the system sizes investigated so far, the integrated difference of the GA is generally smaller than that of the ST. However, the integrated difference of the ST is found to decrease with increasing system size, which is consistent with the result of the AM [13]. Fluctuating with the system size, the integrated difference of the GA does not decay with increasing system size, which implies the non-Gaussian nature of $P_L(\alpha)$ at even large system sizes. Thus, our results suggest that, by increasing the system size of our model, the singularity spectrum $f(\alpha)$ at a ME gets satisfied with the symmetric relation in Eq. (17) but not with the PA in Eq. (13).

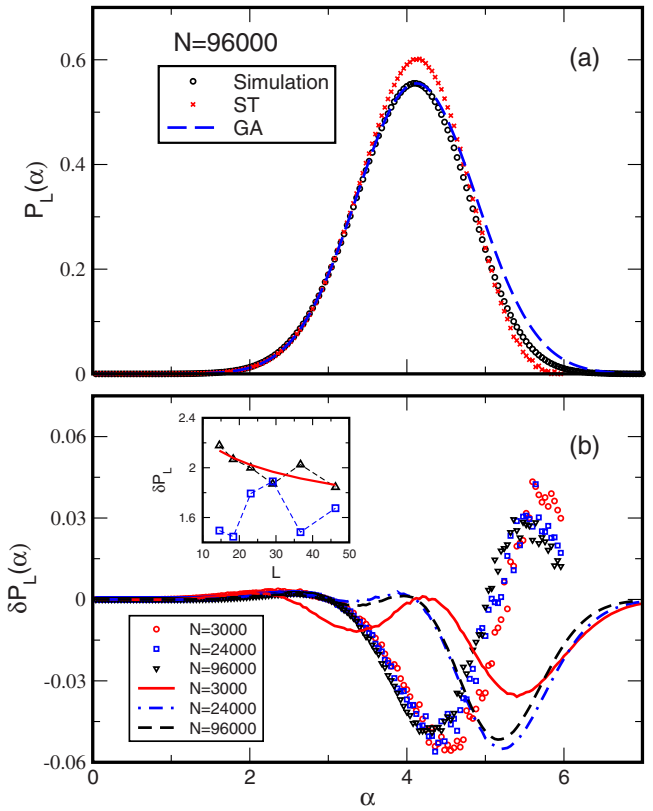

FIG. 8. (Color online) (a) $P_L(\alpha)$ (circles), $P_L^{\mathrm{GA}}(\alpha)$ (dashed line), and $P_L^{\mathrm{ST}}(\alpha)$ (crosses) for $N=96\,000$. (b) For $N=3000$, 24 000, and 96 000, $\delta P_L^{\mathrm{GA}}(\alpha)$ are indicated by solid, dashed-dotted, and dashed lines and $\delta P_L^{\mathrm{ST}}(\alpha)$ are indicated by circles, squares, and triangles, respectively. The inset shows the system-size dependences of δP_L^{GA} (squares) and δP_L^{ST} (triangles). The red solid line is the fit of AL^{-B} for δP_L^{ST}, with $B=0.12$.

C. Spatial correlation function

To characterize the spatial structures of the multifractal INMs, we define the spatial correlation function [41] for the qth moment of the squared vibrational amplitudes of two particles separated at a distance r in a system of size L as

$$C_q(r,L)=\left\langle \frac{1}{N}\sum_{i=1}^{N}\sum_{j\neq i}^{N}|\mathbf{e}_i^s|^{2q}|\mathbf{e}_j^s|^{2q}\delta(r-r_{ij})\right\rangle_{\lambda}, \tag{21}$$

where r_{ij} is the distance between particles i and j, the brackets denote an ensemble average for the multifractal INMs, and r is assumed to be smaller than half of L. Since the distribution of squared vibrational amplitudes relies on the system size, $C_q(r,L)$ not only is a function of the distance between two particles but also depends on L. In terms of ΔN_r, which is the number of particles within a spherical shell between r and $r+\delta r$ about a central particle, the expression of $C_q(r,L)$ is written as

$$C_q(r,L)=\left\langle \frac{1}{N\Delta N_r}\sum_{i=1}^{N}\sum_{j=1}^{\Delta N_r}|\mathbf{e}_i^s|^{2q}|\mathbf{e}_j^s|^{2q}\right\rangle_{\lambda}, \tag{22}$$

where the second summation is subject to those particles within the shell.

Based on the multifractal nature, a scaling argument for the spatial correlation function of the critical states at the Anderson transition has been given [42,43]. By applying the scaling argument for the squared vibrational amplitudes of the multifractal INMs, the scaling behavior of $C_q(r,L)$ is predicted as

$$C_q(r,L)\propto L^{-y_q}\cdot r^{-z_q}, \tag{23}$$

where y_q and z_q, the correlation exponents of the spatial correlation function, are given as

$$y_q=d+\tau_{2q}, \tag{24}$$

$$z_q=d+2\tau_q-\tau_{2q}. \tag{25}$$

By using the PA of τ_q in Eq. (14), y_q and z_q in the PA are expressed as

$$y_q^{\mathrm{PA}}=2\alpha_0 q-4(\alpha_0-d)q^2, \tag{26}$$

$$z_q^{\mathrm{PA}}=2(\alpha_0-d)q^2. \tag{27}$$

To examine whether the correlation exponents of the multifractal INMs follow the predictions of the scaling argument, we calculate $C_q(r,L)$ at the ME in the negative branch for several system sizes. Presented in Fig. 9(a) are the $C_q(r,L)$ of $N=48\,000$ with $0<q<2$ for r less than $L/2$.

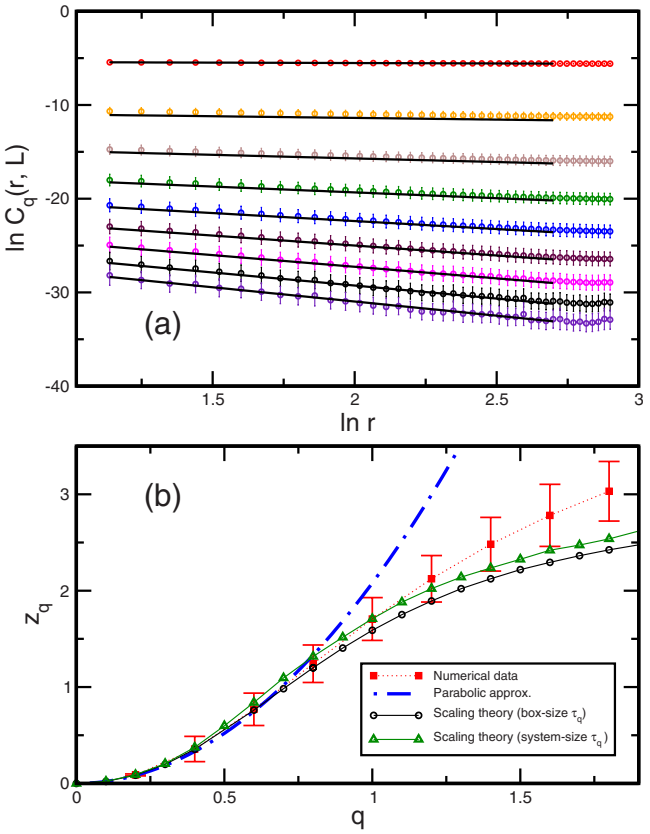

FIG. 9. (Color online) (a) Spatial dependence of $C_q(r,L)$ in a log-log plot for $N=48\,000$. The symbols are the averaged results of INMs with $\lambda=-86.6\pm0.5$. The data from top to bottom are for q from 0.2 to 1.8 with a step of $\Delta q=0.2$. The solid lines are a linear fit for each q. (b) Correlation exponent z_q versus q. The red filled squares are obtained by the linear-fit results in (a). The dashed-dotted line is the PA. The black circles and green triangles are the predictions of the scaling theory with τ_q obtained by the box-size scaling and the system-size scaling, respectively.

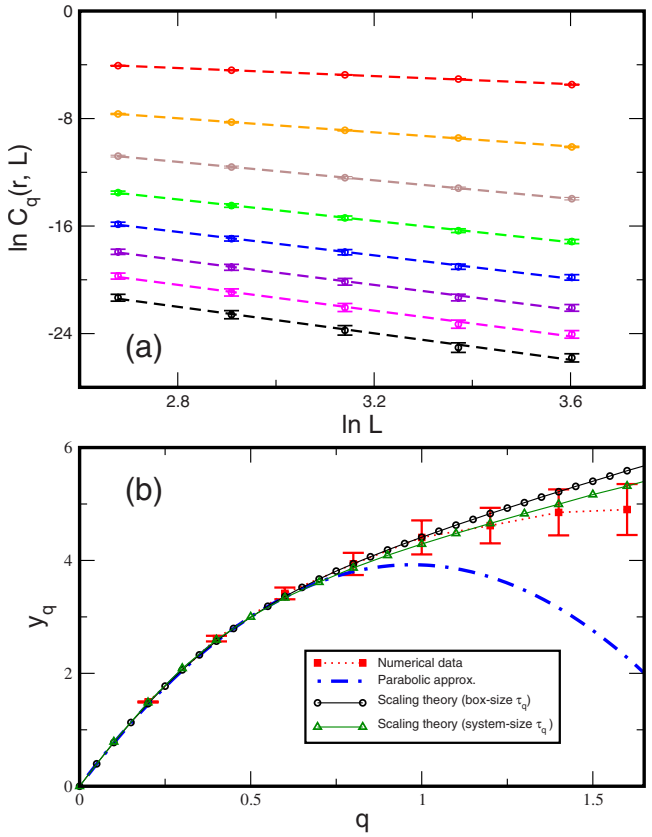

FIG. 10. (Color online) (a) System-size dependence of $C_q(r,L)$ in a log-log plot for an average over r at 4.0, 4.5, 5, and 5.5. The numerical data are for the INMs with $\lambda=-86.6\pm0.5$. From left to right, the system sizes N are from 3000 to 48 000; from top to bottom, the values of q are from 0.2 to 1.6 with a step of $\Delta q=0.2$. The dashed lines are a linear fit for each q. (b) Correlation exponent y_q versus q. The lines and symbols are similar in meaning as those in Fig. 9(b).

Evidenced by our results, $C_q(r,L)$ indeed follows a power-law decay with respect to r. We make a linear fit for the data of each q in Fig. 9(a) so that the data of z_q are extracted. The numerical results of z_q are presented in Fig. 9(b), with the error of z_q estimated by a similar way given in Ref. [19]. For large q, the original data of $C_q(r,L)$ suffer from strong fluctuations, which cause large errors in z_q. By substituting the data of τ_q obtained by the box-size scaling or the system-size scaling into Eq. (25), the predictions of the scaling argument are shown in Fig. 9(b) for comparison. Indicated by our results, the scaling argument with τ_q of the box-size scaling agrees with the numerical data for $q<1$; however, with τ_q of the system-size scaling, the range in q for the agreement is extended up to 1.2. With $\alpha_0=4.04$ in Eq. (25), the PA of z_q is good for $q<0.7$, which is consistent with that the PA for τ_q is only good for small q.

Similarly, we calculate $C_q(r,L)$ at a fixed r for several system sizes of N varying from 3000 to 48 000. No qualitative difference is found in the system-size dependence of $\ln C_q(r,L)$, wherever r is set at 4.0, 4.5, 5, or 5.5, which are distances around the fifth shell in the radial distribution function but still smaller than half of L for $N=3000$. With results averaged for the four distances of r, $\ln C_q(r,L)$ versus $\ln L$ is plotted in Fig. 10(a). The linearity of the data for each q in Fig. 10(a) indicates the power-law dependence of $C_q(r,L)$ with respect to L and the slope of a linear fit gives the numerical data of y_q, which are shown in Fig. 10(b) with the errors estimated in a similar way as those of z_q. We have examined the data of y_q for $\ln C_q(r,L)$ evaluated at the four distances of r; however, the variation of y_q with r is too small to be noticeable. Again, with the τ_q data obtained by the box-size scaling, the prediction of the scaling argument for y_q agrees with the numerical results for $q<1.2$, which is a little larger than that for z_q. Similarly, by the τ_q data of the system-size scaling, the upper limit of the agreement extends to $q=1.4$. However, the PA of y_q in Eq. (26) is still only good for $q<0.7$.

V. CONCLUSIONS

In this paper, we have investigated the multifractality of the INMs at the two MEs of a simple fluid, with the two MEs distinguishable by positive or negative eigenvalue. The locations of the MEs were determined in a previous work by

using the level-spacing statistics and the finite-size scaling [19]. We generalize the multifractal analysis for the INMs at a ME with the box-counting method, in which the simulated system is partitioned into small boxes of equal volumes. Because of the fluidity of our model, the particle numbers in the divided small boxes fluctuate around an average value; this is a major difference between our model and the lattice AM. By means of the multifractal analysis under the typical average, we have calculated the generalized inverse participation ratios of the squared vibrational amplitudes in the INMs by the box-size and system-size scalings. The results of the box-size scaling indicate that the INMs at a ME are characterized in the multifractal nature and the multifractals at the two MEs yield the same results in generalized fractal dimensions and singularity spectrum. By both box-size and system-size scalings, the singularity spectrum of the multifractal INMs agrees well with that of the AM, which provides a numerical evidence for the universal multifractality at the localization-delocalization transition due to disorder.

We have examined the singularity spectrum of the INMs with the symmetric relation originally proposed for the nonlinear σ model [10]. Our results indicate that the symmetric relation is obeyed as our model is in a very large system size; a similar conclusion is also obtained with the AM [11,13]. In principle, multifractals exhibit self-similarity for all length scales, indicating that no length scale is determined by the systems where the multifractals are produced. However, our model and the AM are discrete models with a fundamental length unit, which is the lattice constant in the AM or the particle size in our model. In a length scale comparable with the length unit of a discrete model, the basic assumption of multifractals breaks down for the model. We conjecture that this is the reason why the system sizes of our model and the AM should be extremely large in order that the singularity spectra of the two models are fulfilled with the proposed symmetric relation.

For the multifractal INMs, the PDF of the logarithm of squared vibrational amplitudes is calculated for several system sizes. Associated with the maximum of the singularity spectrum, the location of the maximum PDF is invariant with the system size. For the system sizes we have investigated so far, the PDF of the multifractal INMs is deviated from a Gaussian distribution, which corresponds to the singularity spectrum under the PA, especially in the region for the small vibrational amplitudes. Indicated by our numerical results, the deviation does not decrease with increasing the system size.

The spatial characteristics of the multifractal INMs in a finite-size system are examined by the spatial correlation function for the qth moment of the squared vibrational amplitudes of two particles. Being a function of the two-particle distance and the system size, the spatial correlation function is numerically evidenced to decay in a power law for each variable with a correlation exponent. By a scaling argument [42,43], the two correlation exponents of the spatial correlation function are related to the mass exponents of the multifractal INMs. With the mass exponents obtained by the box-size and system-size scalings, the predications of the scaling argument agree with the numerical results of the two correlation exponents at small q but are deviated at large q; the prediction by the system-size scaling produces a larger range of agreement in q than that of the box-size scaling. The deviation at large q is possibly resulted from the different averages used in our calculations for the spatial correlation function and the mass exponents of the multifractal INMs, which are under the ensemble and typical averages, respectively. The deviation is expected to be improved as the mass exponents of the INMs are also calculated under the ensemble average, which produces better results in the singularity spectrum of the AM than the typical average does [12]. The multifractal analysis for the INMs under the ensemble average will be one of our future works.

ACKNOWLEDGMENTS

We are indebted to Professor R. A. Römer for providing their data of the AM. T.-M.W. acknowledges financial supports from the National Science Council of Taiwan, under Grant No. NSC 99-2112-M-009-003-MY2.

[1] P. W. Anderson, Phys. Rev. **109**, 1492 (1958).
[2] F. Evers and A. D. Mirlin, Rev. Mod. Phys. **80**, 1355 (2008).
[3] J. Billy, V. Josse, Z. Zuo, A. Bernard, B. Hambrecht, P. Lugan, D. Clement, L. Sanchez-Palencia, P. Bouyer, and A. Aspect, Nature (London) **453**, 891 (2008).
[4] G. Roati, C. D'Errico, L. Fallani, M. Fattori, C. Fort, M. Zaccanti, G. Modugno, M. Modugno, and M. Inguscio, Nature (London) **453**, 895 (2008).
[5] H. Hu, A. Strybulevych, J. H. Page, S. E. Skipetrov, and B. van Tiggelen, Nat. Phys. **4**, 945 (2008).
[6] A. Lagendijk, B. van Tiggelen, and D. S. Wiersma, Phys. Today **62**(8), 24 (2009).
[7] A. Aspect and M. Inguscio, Phys. Today **62**(8), 30 (2009).
[8] A. Richardella, P. Roushan, S. Mack, B. Zhou, D. A. Huse, D. D. Awschalom, and A. Yazdani, Science **327**, 665 (2010).
[9] M. Schreiber and H. Grussbach, Phys. Rev. Lett. **67**, 607 (1991).
[10] A. D. Mirlin, Y. V. Fyodorov, A. Mildenberger, and F. Evers, Phys. Rev. Lett. **97**, 046803 (2006).
[11] L. J. Vasquez, A. Rodriguez, and R. A. Römer, Phys. Rev. B **78**, 195106 (2008).
[12] A. Rodriguez, L. J. Vasquez, and R. A. Römer, Phys. Rev. B **78**, 195107 (2008).
[13] A. Rodriguez, L. J. Vasquez, and R. A. Römer, Phys. Rev. Lett. **102**, 106406 (2009).
[14] W. Garber, F. M. Tangerman, P. B. Allen, and J. L. Feldman, Philos. Mag. Lett. **81**, 433 (2001).
[15] J. J. Ludlam, S. N. Taraskin, and S. R. Elliott, Phys. Rev. B **67**, 132203 (2003).
[16] J. L. Feldman and N. Bernstein, Phys. Rev. B **70**, 235214 (2004).
[17] J. J. Ludlam, S. N. Taraskin, S. R. Elliott, and D. A. Drabold,

J. Phys.: Condens. Matter **17**, L321 (2005).
[18] S. Faez, A. Strybulevych, J. H. Page, A. Lagendijk, and B. A. van Tiggelen, Phys. Rev. Lett. **103**, 155703 (2009).
[19] B. J. Huang and T. M. Wu, Phys. Rev. E **79**, 041105 (2009).
[20] R. M. Stratt, Acc. Chem. Res. **28**, 201 (1995).
[21] M. L. Mehta, *Random Matrices* (Academic Press, San Diego, 1991).
[22] A. Chhabra and R. V. Jensen, Phys. Rev. Lett. **62**, 1327 (1989).
[23] T. M. Wu, W. J. Ma, and S. F. Tsay, Physica A **254**, 257 (1998).
[24] T. M. Wu and R. F. Loring, J. Chem. Phys. **97**, 8568 (1992).
[25] M. Bollhöfer and Y. Notay, Comput. Phys. Commun. **177**, 951 (2007).
[26] O. Schenk, M. Bollhöfer, and R. A. Römer, SIAM J. Sci. Comput. (USA) **28**, 963 (2006).
[27] B. J. Huang and T. M. Wu, Comput. Phys. Commun. **182**, 213 (2011), doi: 10.1016/j.cpc.2010.07.015
[28] T. M. Wu and W. J. Ma, J. Chem. Phys. **110**, 447 (1999).
[29] T. Nakayama and K. Yakubo, *Fractal Concepts in Condensed Matter Physics* (Springer-Verlag, Berlin, 2003).
[30] A. D. Mirlin and F. Evers, Phys. Rev. B **62**, 7920 (2000).
[31] D. A. Parshin and H. R. Schober, Phys. Rev. B **57**, 10232 (1998).
[32] T. Terao, Phys. Rev. B **56**, 975 (1997).
[33] D. A. Parshin and H. R. Schober, Phys. Rev. Lett. **83**, 4590 (1999).
[34] E. Cuevas, M. Ortuño, V. Gasparian, and A. Pérez-Garrido, Phys. Rev. Lett. **88**, 016401 (2001).
[35] A. Mildenberger, F. Evers, and A. D. Mirlin, Phys. Rev. B **66**, 033109 (2002).
[36] A. Rodriguez, L. J. Vasquez, K. Slevin, and R. A. Römer, Phys. Rev. Lett. **105**, 046403 (2010).
[37] F. Wegner, Nucl. Phys. B **316**, 663 (1989).
[38] A. D. Mirlin and Y. V. Fyodorov, J. Phys. I **4**, 655 (1994).
[39] D. V. Savin, H. J. Sommers, and Y. V. Fyodorov, JETP Lett. **82**, 544 (2005).
[40] A. Mildenberger and F. Evers, Phys. Rev. B **75**, 041303 (2007).
[41] M. E. Cates and J. M. Deutsch, Phys. Rev. A **35**, 4907 (1987).
[42] K. Pracz, M. Janssen, and P. Freche, J. Phys.: Condens. Matter **8**, 7147 (1996).
[43] H. Obuse and K. Yakubo, J. Phys. Soc. Jpn. **73**, 2164 (2004).